This is a “preproof” accepted article for *Mineralogical Magazine*.
This version may be subject to change during the production process.
10.1180/mgm.2025.6

Crystal structure and high-temperature transformation of $RbAlGe_3O_8$, a germanium analogue of rubicline, $RbAlSi_3O_8$

Liudmila A. Gorelova[1*], Maria G. Krzhizhanovskaya[1], Valentina A. Yukhno[1], Olga Yu. Shorets[2], Oleg S. Vereshchagin[1]

Corresponding author: *l.gorelova@spbu.ru

[1] Saint Petersburg State University, Universitetskaya Emb. 7/9, 199034 St. Petersburg, Russia.

[2] Grebenshchikov Institute of Silicate Chemistry, Makarova nab. 2, 199034 St. Petersburg, Russia

Abstract

Rubicline, $RbAlSi_3O_8$, is one of three known minerals containing essential rubidium and a geochemically significant member of the feldspar family. In the course of current work, $RbAlGe_3O_8$ (germanium analogue of rubicline) was grown hydrothermally via the formation of leucite-like $RbAlGe_2O_6$ as an intermediate phase. The crystal structure of $RbAlGe_3O_8$ was determined for the first time by direct methods from single crystal X-ray diffraction data and refined to R_1 = 0.0528. It has monoclinic symmetry (space group $C2/m$, a = 9.1237(9), b = 13.5679(6), c = 7.4677(4) Å, β = 116.687(6)°, V = 825.95(11) Å^3), with cell parameters typical for disordered feldspars. According to the high temperature study, feldspar-like $RbAlGe_3O_8$ irreversibly transforms into the leucite-like phase $RbAlGe_2O_6$ at 1050 °C. The thermal expansion

https://doi.org/10.1180/mgm.2025.6 Published online by Cambridge University Press

of studied material displays a small negative change along the *b* axis. Its volume thermal expansion, fitted according to a linear model between 30 and 840 °C (α_V = 20.3(1) ×10^{-6} °C^{-1}), is slightly higher than that of other feldspar-related compound with essential rubidium.

Keywords: $RbAlGe_3O_8$; $RbAlGe_2O_6$; feldspar; leucite; thermal expansion; crystal structure;

1. Introduction

Feldspars are among the most widespread minerals in the terrestrial planets and form about 50 wt. % of the Earth's crust and a significant part of the Moon's crust (e.g., Ohtake *et al*. 2009; Vadawale *et al*. 2024). Most widespread in nature are alkaline aluminosilicate feldspars, such as microcline, orthoclase, sanidine ($KAlSi_3O_8$) and albite ($NaAlSi_3O_8$). Countless works have been devoted to their study, including handbooks, monographs and reviews (e.g. Smith and Brown, 1988; Angel, 1994; Deer *et al*., 2001; Bokiy and Borutzky, 2003; Krivovichev, 2020). Interest in their study is associated not only with their geological significance, but also due to the wide application in various industries (e.g. Carter and Norton, 2008; Zhang *et al.,* 2018; Silva *et al.,* 2019; Fuertes *et al.*, 2022). In addition, feldspars are among the most important mineral-sources of rubidium (e.g. Greenwood and Barnshaw, 1998; Xing *et al.*, 2018).

Despite the relatively high concentrations of rubidium in the Earth's crust (90 ppm by mass; Christy, 2015), minerals with essential rubidium are extremely rare in nature (mindat; Ralph *et al*., 2024). The geochemical similarity of rubidium to potassium leads to the fact that this element is scattered and, unlike other alkali metals, almost all rubidium is dispersed between feldspars, leucite - pollucite and mica (e.g. Solodov *et al.*, 1980). Nevertheless, according to the list of minerals accepted by the International Mineralogical Association (IMA), to date 3 mineral species with essential rubidium are known: ramanite-(Rb) $RbB_5O_6(OH)_4{\cdot}2H_2O$ (Rainer *et al.*, 2008), voloshinite $Rb(LiAl_{1.5}\square_{0.5})(Al_{0.5}Si_{3.5})O_{10}F_2$ (Pekov *et al.*, 2009) and rubicline $RbAlSi_3O_8$

https://doi.org/10.1180/mgm.2025.6 Published online by Cambridge University Press

(Teertstra *et al.*, 1998a). It is worth noting, that all three of them were found in granitic pegmatites and 2 out of 3 are Rb analogues of rock-forming minerals. It is also interesting to note that all three Rb-minerals are usually formed in association with pollucite (Teertstra *et al.*, 1997, 1998a, 1999a; Rainer *et al.*, 2008; Pekov *et al.*, 2009). Rubicline, the first approved and the most widespread rubidium mineral, is a rubidium analogue of microcline, i.e. belongs to the feldspar family and is usually found in granitic pegmatites (Teertstra *et al.*, 1997, 1998a, 1999a; Krivovichev, 2020).

Due to the resemblance of physical properties of Si (Z = 14) and Ge (Z = 32), for many years, germanium analogues of rock-forming silicates have been synthesized in order to determine their properties at lower pressure-temperature (PT) conditions and thus to simulate the possible mineral structure types of the Earth's interior (e.g. Kume *et al.*, 1966, 1969; Ringwood *et al.*, 1967; Ahrens *et al.*, 1969; Kinomura *et al.*, 1971; Kovalev *et al.*, 2024). Though Ge is a trace element in the Earth's crust, it tends to substitute Si in rock-forming minerals (e.g., Goldschmidt, 1926, 1958). Besides, Ge/Si ratio in different natural environments is an important tracer of silicate weathering and secondary mineral formation (e.g., De Argollo and Schilling, 1978; Bernstein, 1985; Mortlock and Frohlich, 1987; Murnane and Stallard, 1990). The most important minerals for evaluation of such processes are feldspars (e.g., Froelich *et al.*, 1992; Kurtz *et al.*, 2002; Baronas *et al.*, 2018). From a material science point of view, the substitution of Ge for Si influences the properties of ion exchange, catalysis, molecular sieving etc. (e.g. Breck, 1974; Lerot *et al.*, 1975; Corma *et al.*, 1990; Helliwell *et al.*, 1993). Besides, some works demonstrate that Ge addition during the synthesis of silicates (e.g. zeolites) lead to enhance the rate of its nucleation and growth (e.g. Cheng *et al.*, 2006); the partial substitution of Si to Ge can lead to improving the efficiency, thermal stability of the luminescent properties, lowering of the sintering temperature and improvement of dielectric properties of some compounds (e.g. Suzuki *et al.*, 2015; Zhang *et al.*, 2022; Appiah *et al.*, 2024). Nevertheless, differences in the atomic radii of Si and Ge (0.26 and 0.39 Å, respectively; Shannon, 1976) leads to the formation of new

https://doi.org/10.1180/mgm.2025.6 Published online by Cambridge University Press

crystal structures, which have no silicate analogues (e.g. Li and Yaghi, 1998; O'Keeffe and Yaghi, 1999).

To date only three 'ternary' compounds are known in the Rb_2O–Al_2O_3–GeO_2 system: $RbAlGe_3O_8$ (Kinomura *et al.*, 1971; Tripathi and Parise, 2002), $RbAlGe_2O_6$ (Torres-Martinez and West, 1989; Bell, 2024) and $RbAlGeO_4$ (Kivlighn, 1966; Terry *et al.*, 2022). According to published data $RbAlGe_2O_6$ has a pollucite-like structure, $RbAlGeO_4$, most probably, can crystallize with triclinic tridymite-like structure (Terry *et al.*, 2022) or with tetragonal symmetry (Kivlighn, 1966). $RbAlGe_3O_8$ is known in three different polymorphic modifications: feldspar-, hollandite- and paracelsian-like (Kinomura *et al.*, 1971; Tripathi and Parise, 2002). Note that only approximate values of the unit-cell parameters were provided for feldspar-like and hollandite-like $RbAlGe_3O_8$ and no crystal structures were obtained for these polymorphs.

The present study is aimed at characterizing the crystallization process, crystal structure and high-temperature behaviour of $RbAlGe_3O_8$ with feldspar topology using single crystal X-ray diffraction (SCXRD) and *in situ* high-temperature (HT) powder X-ray diffraction (PXRD) up to 1110 ºC in order to determine its crystal structure, thermal expansion and transformation and compare it with the previously studied isostructural compounds.

2. Materials and methods

2.1. Synthesis, phase and chemical composition

$RbAlGe_3O_8$ was synthesized from chemically pure Rb_2CO_3 (99.99%, Sigma-Aldrich), Al_2O_3 (99.99 %, Sigma-Aldrich) and GeO_2 (99.99%, Sigma-Aldrich), taken in the mole ratios of 0.5:0.5:3, respectively. The reagents were ground in an agate mortar and placed in a platinum crucible. The mixture was heated in air at 600, 900 and 1000 °C (Table 1). After heating, the sample was transferred to a Teflon liner containing distilled water. The liner was sealed and

https://doi.org/10.1180/mgm.2025.6 Published online by Cambridge University Press

placed in an autoclave, which was then heated in an oven at 220 °C for 7 days (sat vapor pressure about 3 MPa) before cooling to room temperature.

The phase composition of all synthesized samples was determined by PXRD using a MiniFlex II (Rigaku Oxford Diffraction, Japan) X-ray diffractometer (Cu*K*α_{1+2} radiation, 30 kV / 15 mA, Bragg-Brentano geometry, DTEX/ULTRA). The chemical composition of the obtained compounds was determined using a S-3400 N scanning electron microscope (Hitachi, Japan) equipped with an AzTec Energy 350 energy dispersive (EDX) spectrometer (Oxford Diffraction, UK) (Supplementary Tables S1).

Table 1. Synthesis conditions and resulting phase composition

No	Heat treatment: T (°C) / time (h)	Resulting phase composition (PXRD data)
1	600 / 10	$RbAlGe_2O_6$, GeO_2, $Rb_2Ge_4O_9$
2	600 / 10 + 900 / 5	$RbAlGe_2O_6$, GeO_2, Al_2O_3
3	600 / 10 + 900 / 20	$RbAlGe_2O_6$, $Rb_2Ge_8O_{17}$
4	600 / 10 + 900 / 20 + 1000 / 24	$RbAlGe_2O_6$, Rb_2O, GeO_2, $Rb_6Ge_2O_7$
5	600 / 10 + 900 / 20 + 1000 / 24 + 220 / 168 (in autoclave)	$RbAlGe_3O_8$

2.2. Single crystal X-ray diffraction (SCXRD)

The SCXRD analysis of $RbAlGe_3O_8$ was performed using a XtaLAB Synergy-S (Rigaku, Japan) diffractometer equipped with an HyPix-6000HE detector (Mo*K*α radiation, 50 kV, 1 mA). The single crystal of $RbAlGe_3O_8$ with the approximate size of 10 × 10 × 10 μm was mounted on a glass fiber using paraton-*n*. The obtained SCXRD data were integrated and corrected for background, Lorentz, and polarization effects. An empirical absorption correction based on the spherical harmonics implemented in the SCALE3 ABSPACK algorithm was applied in the CrysAlisPro program (Agilent, 2012). The unit-cell parameters were refined using the least-square techniques. The SHELXL program package (Sheldrick, 2008) was used for all structural calculations (Supplementary Tables S2 and S3).

https://doi.org/10.1180/mgm.2025.6 Published online by Cambridge University Press

2.3. High-temperature powder X-ray diffraction (HT PXRD)

The HT behavior of all studied compounds (see below) has been performed under heating in air by HT PXRD using an Ultima IV (Rigaku, Japan) diffractometer (Cu*K*α radiation, 40 kV / 30 mA, Bragg-Brentano geometry, PSD D-Tex Ultra detector) with a thermo-attachment in the range 30–1110 °C with the temperature steps of 30 °C. The fine-powdered sample was deposited on a platinum sample holder (20 × 12 × 1.5 mm) from an ethanol suspension (Filatov, 1971). An external Si standard was used before the measurements to control the 2θ correctness and peaks from platinum sample holder were used as internal standard during experiment. The calculations of the unit-cell parameters were performed using the program package Topas 4.2 (Dinnebier *et al.*, 2019). The temperature dependence of the unit-cell parameters was described by linear functions. The calculation and visualization of the thermal expansion parameters tensor was performed using the TTT program package (Bubnova *et al.*, 2013).

3. Results and discussion

3.1. Formation of $RbAlGe_3O_8$

The solid state synthesis method does not lead to formation of $RbAlGe_3O_8$ (Table 1). All the heat treatment leads to the formation of $RbAlGe_2O_6$ leucite-like phase (*I*–43*d* space group (sp.gr.); PDF 00-037-0348) with admixture of different phases. Such results are in agreement with alkali aluminosilicate feldspars ($M^+AlSi_3O_8$) being difficult to nucleate and grow from their anhydrous melts (Schairer and Bowen, 1955; Kirkpatrick *et al.*, 1979; McMillan, 1979; Taylor and Brown, 1979; Smith and Brown, 1988; Liu *et al.*, 1994) and it is much easier to synthesize

https://doi.org/10.1180/mgm.2025.6 Published online by Cambridge University Press

alkali feldspar crystals using hydrothermal methods (e.g., Barrer and McCallum, 1953; Barrer and Baynham, 1956).

Thus, hydrothermal synthesis leads to the formation of $RbAlGe_3O_8$, whose powder XRD pattern is similar to the compound described by Kinomura et al. (1971). Considering the low symmetry of the obtained compound and the presence of single crystals, the crystal structure of $RbAlGe_3O_8$ has been studied and refined using SCXRD data (see below). Chemical analysis of the obtained compound showed that it is stoichiometric (Rb:Al:Ge 1:1:3) and does not contain impurities in quantities determined by the EDX (> 0.1 wt. %; Electronic Supplementary Material Table S1).

As mentioned above, $RbAlGe_3O_8$ has been obtained during hydrothermal synthesis at a temperature 220 °C. The formation conditions of its aluminosilicate analog, rubicline, are very close in hydrothermal conditions, where it can form at 250–150 °C (Teertstra *et al.*, 1999b). Also note that rubicline is usually found as a dispersed phase in pollucite, $(Cs,Na)_2(Al_2Si_4O_{12})\cdot 2H_2O$ or microcline (e.g. Teertstra *et al.*, 1997, 1998a; Pekov *et al.*, 2009). Synthetic rubicline and its analogue $RbGaSi_3O_8$ can be obtained hydrothermally at 0.1 GPa and 500 or 600 °C, respectively (Henderson, 2021). In other words, the formation pathway of synthetic $RbAlGe_3O_8$ is close to that of rubicline.

3.2. Crystal structure of $RbAlGe_3O_8$ under ambient conditions and its comparison with other feldspar-related compounds

The crystal structure of the $RbAlGe_3O_8$ was refined in *C*2/*m* space group (Table 2), which is typical for disordered modifications of alkaline feldspars and their synthetic analogs (e.g. Colville and Ribbe, 1968; Gasperin, 1971; Kimball and Megaw, 1974; Winter *et al.*, 1979; Kroll and Ribbe, 1987; Kroll *et al.*, 1991). The similar type of Ge / Al disordering has been also observed for $RbAlGe_3O_8$ with paracelsian topology (Tripathi and Parise, 2002). The crystal

https://doi.org/10.1180/mgm.2025.6 Published online by Cambridge University Press

structure of the third known modification of $RbAlGe_3O_8$ (with hollandite topology) is characterized by the unit-cell parameters only (Kinomura *et al.*, 1971).

The crystal structure of studied $RbAlGe_3O_8$ can be described by analogy with other feldspar-related compounds, i.e. as three-dimensional framework, consisting of corner-sharing TO_4 tetrahedra (T = Al, Ge) (Figures 1a-c). According to the symmetry and chemical composition, there are two independent tetrahedrally coordinated sites, which are occupied by statistically distributed Ge and Al with the 3:1 ratio that is confirmed by the similar bond lengths in both tetrahedra (Table S3). Rb atoms, located in the framework cavities, are coordinated by ten oxygen atoms with the average bond length 3.156 Å (Table S2). Connected *via* edges, the RbO_{10} polyhedra form infinite chains along the [101] direction (Figure 1d).

Table 2. Crystallographic data on some feldspar-related compounds with feldspar topology

Composition	$RbAlGe_3O_8$	$RbAlSi_3O_8$	$RbGaSi_3O_8$	$KAlGe_3O_8$	$KAlSi_3O_8$	$KGaSi_3O_8$	$KBSi_3O_8$	$NaAlSi_3O_8$	$LiAlSi_3O_8$
a, Å	9.1237(9)	8.839(2)	8.919	8.8163(5)	8.603(2)	8.660(1)	8.4377(8)	8.274(5)	7.859(2)
b, Å	13.5679(6)	13.035(2)	13.089	13.5536(6)	13.036(4)	13.102(2)	12.4152(11)	12.991(6)	12.659(3)
c, Å	7.4677(4)	7.175(2)	7.254	7.4577(4)	7.174(2)	7.229(1)	6.8769(7)	7.144(4)	7.039(2)
β, °	116.687(6)	116.11(1)	116.43	115.898(1)	116.03(2)	116.06(1)	116.133(7)	116.13(4)	116.72(2)
Volume, Å^3	825.95(11)	742.3(3)	758.3	801.65	722.94	736.84	646.75	689.41	6209(2)
Reference	This study	Kyono and Kimata 2001	Henderson 2021	Kroll et al. 1991	Ferguson et al. 1991	Kimata et al. 1995	Krzhizhanovskaya *et al.*, 2012	Winter et al. 1979	Hovis et al., 2008

https://doi.org/10.1180/mgm.2025.6 Published online by Cambridge University Press

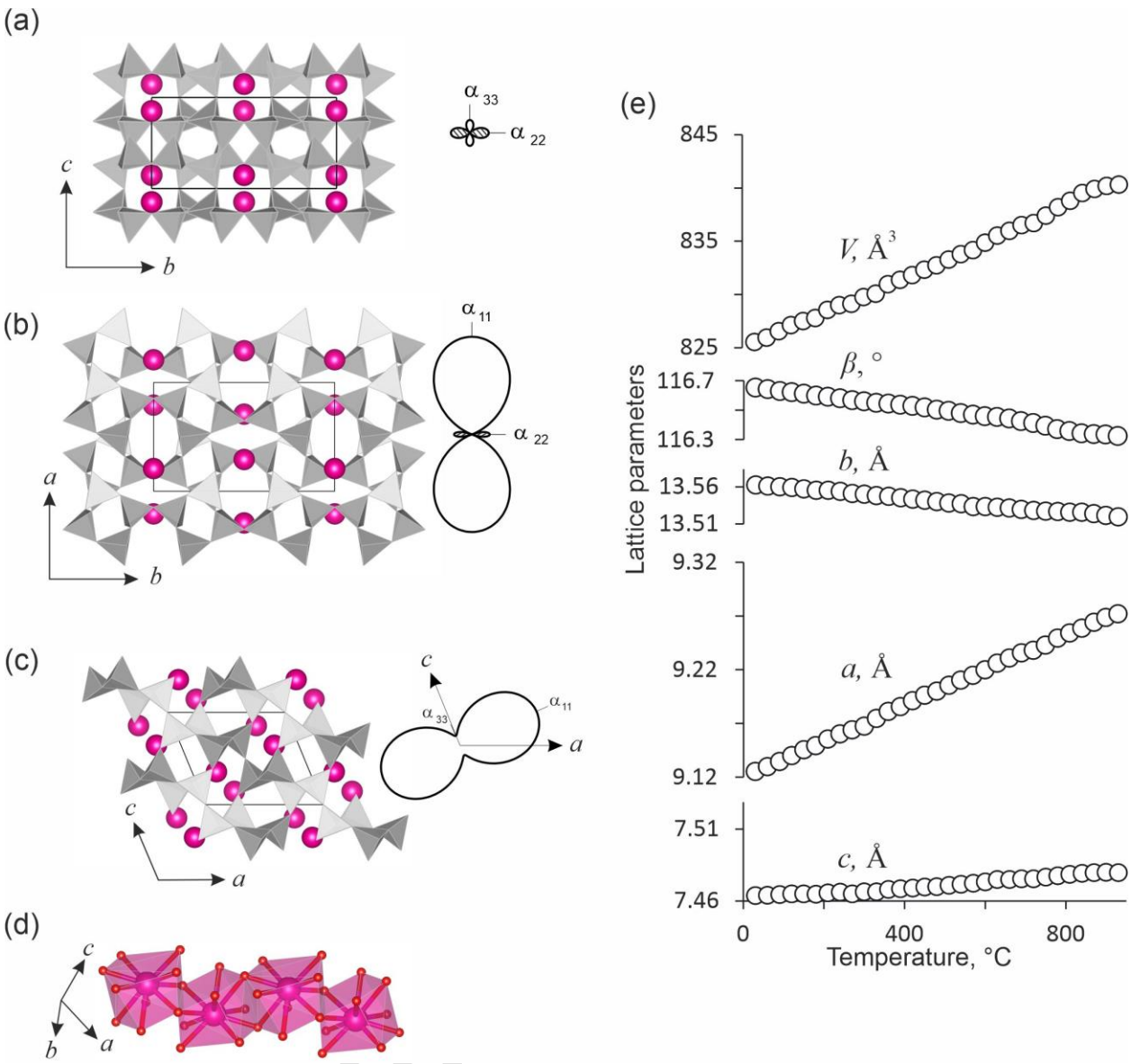

Figure 1. Crystal structure of $RbAlGe_3O_8$ with feldspar topology with averaged thermal expansion section (dashed part of the sections demonstrate the negative thermal expansion) in different projections (a–c); chain of RbO_{10} polyhedra (d) and unit-cell parameters of $RbAlGe_3O_8$ at different temperatures (e). $(Al,Ge)O_4$ tetrahedra are given in grey, Rb and O atoms are shown as pink and red spheres, respectively. Errors are smaller than symbols.

Among natural feldspars, the studied $RbAlGe_3O_8$ is closest to rubicline in chemical composition (Teertstra *et al.*, 1997, 1998a; c). Natural rubicline is crystallized in triclinic symmetry (*C*–1 space group), with an ordered crystal structure (Teertstra *et al.*, 1998c) and

https://doi.org/10.1180/mgm.2025.6 Published online by Cambridge University Press

occurs in granitic pegmatites; there are also data on possible crystallization of disordered rubicline in metasomatic rocks (e.g. Teertstra *et al.*, 1998b). Interestingly, synthetic analogues of rubicline can crystallize both in ordered (*C*–1) (Wietze and Wiswanathan, 1971; Grove and Ito, 1973; McMillan *et al.*, 1980) and as Al/Si-disordered (*C*2/*m*) modifications (Barrer and McCallum, 1953; Ghelis and Gasperin, 1970; Gasperin, 1971; Pentinghaus and Bambauer, 1971; Bruno and Pentinghaus, 1974; Voncken, 1996; Kovalskii *et al.*, 2000; Kyono and Kimata, 2001). The disordered modification (with monoclinic symmetry) is more typical for 'high-temperature' feldspars, whereas 'low-temperature' feldspars are usually ordered and have triclinic symmetry (Deer *et al.*, 2013). It should be also noted, that other alkaline feldspar minerals with feldspar topology, such as $NaAlSi_3O_8$ and $KAlSi_3O_8$ are also known in both ordered and disordered forms (e.g. Winter *et al.*, 1979; Kroll and Ribbe, 1987), whereas their synthetic Ge- and Ga-analogues are forming in disordered modifications only (Kroll *et al.*, 1991; Kimata *et al.*, 1995). This relationship is probably related to the long duration of geological processes compared to laboratory experiments.

The volume of the unit-cell of alkaline feldspars is determined more by the size of framework-forming (*T*) cations, than by size of extraframework (*M*) cations (Figure 2a and b), i.e. from the crystallographic point of view, $RbAlGe_3O_8$ is most close to $KAlGe_3O_8$, with unit cell volumes >800 $Å^3$ (Table 2). A similar tendency is observed not only for volume, but also for *b* and *c* parameters, whereas *a* parameters are more influenced by the *M* cation (Figure 2c). It is also interesting to note that $RbAlGe_3O_8$ has the maximal β angle among other alkaline feldspars (Table 2, Figure 2f). These features reflect the significant flexibility of the framework with feldspar topology (Smith, 1958, 1974).

https://doi.org/10.1180/mgm.2025.6 Published online by Cambridge University Press

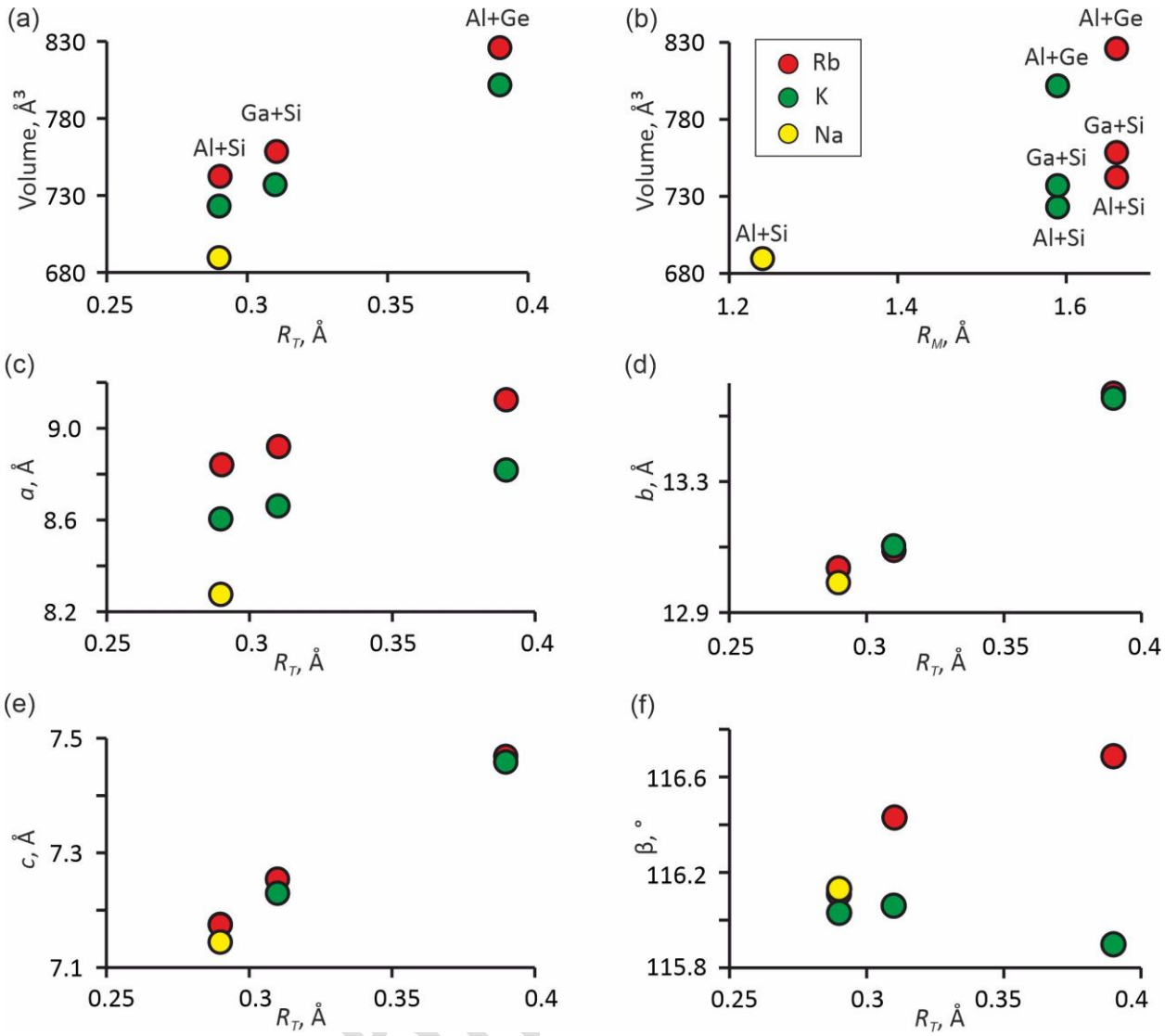

Figure 2. Crystal chemical aspects of alkaline feldspar-related compounds with different chemical composition: dependence of the volume of the unit-cell on radii ($R_T = (R_{T1}+3R_{T2})/4$) of tetrahedrally coordinated cations (*T*) (a) and on radii of extraframework cations (*M*) (b); dependence of the unit-cell parameters on radii ($R_T = (R_{T1}+3R_{T2})/4$) of tetrahedrally coordinated cations (*T*) (c-f).

3.3. Temperature behavior of $RbAlGe_3O_8$ and its analogues with feldspar topology

The temperature evolution (in the range 30–1110 ºC) of the diffractions peaks of feldspar-like $RbAlGe_3O_8$ is given in Figure 3. The experiment demonstrates that above 930 ºC $RbAlGe_3O_8$ starts to decompose according to the reaction: $RbAlGe_3O_8 \rightarrow RbAlGe_2O_6 + GeO_2$,

https://doi.org/10.1180/mgm.2025.6 Published online by Cambridge University Press

where $RbAlGe_2O_6$ is a leucite-like phase (PDF 00-037-0348). The feldspar-like phase disappears completely above 1050 ºC (Figure 3). The leucite-like phase has cubic symmetry (*I*–43*d*; *a* = 14.0535(2) Å, *V* = 2775.6(1) Å^3) at 1080 °C, that is a good agreement with previously obtained data (*I*–43*d*; *a* = 13.7153(5) Å, *V* = 2579.97(26) Å^3) for the compound at ambient temperature (Bell, 2024).

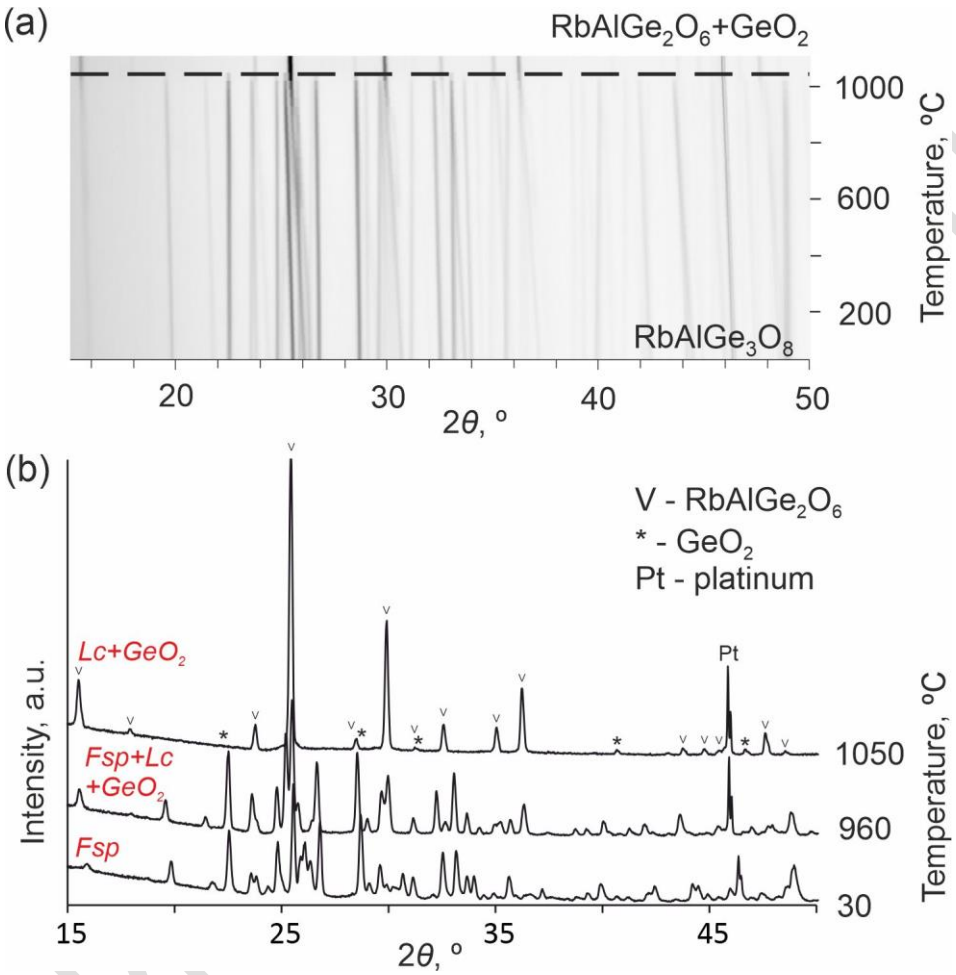

Figure 3. The evolution of the PXRD patterns of $RbAlGe_3O_8$ in the range 30–1110 ºC (a) and at 30, 960 and 1050 ºC (b). *Fsp* – $RbAlGe_3O_8$, *Lc* – leucite-pollucite like phase $RbAlGe_2O_6$.

The transformation of $RbAlGe_3O_8$ into leucite-pollucite like phase ($RbAlGe_2O_6$) is not unexpected, as a similar transformation is known for other K- and Rb-aluminosilicate alkali feldspar solid solutions to single phase leucites (e.g. Henderson *et al.*, 2017). However, depending on the chemical composition of the initial phase, the transformation temperature

https://doi.org/10.1180/mgm.2025.6 Published online by Cambridge University Press

increases with increasing of K content (Henderson *et al.*, 2017, their Figure 2). Note that end-member $RbAlSi_3O_8$ monoclinic alkali feldspar changed above 1000 ^oC to a leucite-type structure (Henderson, 2021).

The temperature dependencies for the unit-cell parameters of $RbAlGe_3O_8$ with feldspar topology before its phase transformation into leucite-like phase are shown in Figure 1e. The thermal expansion of $RbAlGe_3O_8$ with feldspar topology has sharply anisotropic character with the *b* axis showing a small decrease, while maximum expansion is observed for the *a* axis (Table 3, Figure 1). This thermal behavior of *b* parameter (with negative thermal expansion) is specifically typical for Rb-bearing feldspars, while almost all other feldspars (with alkaline extraframework cations) demonstrate the positive thermal expansion along *b* axis (Brown *et al.*, 1984). Notably, published data demonstrate that there are some exception from this rule: microcline (ordered $KAlSi_3O_8$) and $LiAlSi_3O_8$ demonstrate the negative TECs in this direction (Table 3). One more exception from this rule is filatovite, $K(Al,Zn)_2(As,Si)_2O_8$, which demonstrate the negative thermal expansion along *b* axis (α_b = –1.2(1) $\times 10^{-6}$ $°C^{-1}$; Gorelova *et al.*, 2024). Negative thermal expansion is found also along the *c* axis below room temperature in albite (Tribaudino *et al.*, 2011) and that the thermal expansion ellipsoid, calculated from the thermal expansion tensor, shows one axis of negative expansion in plagioclase (Tribaudino *et al.*, 2010). It is interesting to note that the direction of maximal thermal expansion is close to the direction of the minimal thermal vibration of Rb atoms. Such a behavior intuitively seems illogical, but is typical for alkaline feldspars (e.g. Filatov, 1990; Gorelova *et al.*, 2024). That means that for feldspar-like compounds thermal expansion does not depend on expansion of the *M*–O bonds (Brown *et al*., 1984). For a long time it was believed that the anisotropy of feldspars is explained by the straightening of the crankshaft chains (Megaw, 1974), which leads to the high thermal expansion coefficients along these chains, which is usually located along a direction close to the (100) plane normal (Tribaudino *et al*., 2010). Later, Brown *et al*. (1984) demonstrated that strong anisotropy is caused by tilting and rotating of rigid TO_4 tetrahedra. The

https://doi.org/10.1180/mgm.2025.6 Published online by Cambridge University Press

development of this idea leads to the conclusion that the main reason for such anisotropy lies in the topology of the tetrahedral framework (Angel *et al.*, 2012). The high-temperature behaviour of $RbAlGe_3O_8$ is one more example, confirming trends suggested for all alkaline feldspars.

Table 3. Thermal expansion coefficients (TECs) ($\times 10^6$ °C^{-1}) of feldspars and feldspars-like synthetic phases with alkaline cations at different temperatures

Compound	**ΔT, °C**	**TECs along the principle axes of the thermal expansion tensor**				**TECs along the crystallographic axes**						**Volume TECs**	**Reference**
		α_{11}	α_{22}	α_{33}	$\mu_{(\alpha 33 \wedge c)}$	α_a	α_b	α_c	α_α	α_β	α_γ	α_V	
$RbAlGe_3O_8$ (d)	30–840	21.4(1)	-3.7(1)	2.6(1)	24.4(1)	18.18(8)	-3.70(4)	2.6(1)	–	-3.10(6)	–	20.3(1)	This work
$RbAlSi_3O_8$ (d)	20–905	17.4(5)	-2.7(2)	1.1(3)	32.9(2)	12.6(5)	-2.6(2)	1.3(3)	–	-4.6(2)	–	15.9(2)	Henderson 2021***
$RbAlSi_3O_8$ (d)	22–600	18.2(7)	-2.0(1)	0.5(8)	4.4(6)	13.6(7)	-2.0(1)	0.6(8)	–	-4.5(6)	–	17(1)	Hovis *et al.*, 2008***
$RbAlSi_3O_8$ (d)	20–1000	17.4(5)	-2.7(2)	1.1(3)	6.5(2)	12.6(5)	-2.6(2)	1.3(3)	–	-4.6(2)	–	15.9(2)	Henderson 1978***
$RbAlSi_3O_8$ (o)	30–1000	18.7(9)	-3.8(3)	0.9(3)	3.3	14.8(9)	-3.7(3)	0.9(2)	0.3(3)	-3.9(3)	0.2(3)	16(1)	Hovis *et al.*, 2008***
$RbGaSi_3O_8$ (d)	20–1000	16.4(2)	-2.5(2)	1.8(2)	33.8(1)	11.9(2)	-2.5(2)	2.0(2)	–	-4.24(9)	–	15.8(3)	Henderson 2021***
$KAlSi_3O_8$ (d)	20–1000	19.3	0.5	0.4	26	15.3	-0.6	-0.1	–	20.1	–	17.2	Henderson 2021
$KAlSi_3O_8$ (o)	22–1005	19.4(6)	-2.0(3)	0.1(3)	13.0(3)	16.7(6)	-1.8(3)	0.2(3)	0.4(3)	-2.4(3)	2.0(2)	17.5(7)	Henderson 1978***
$KBSi_3O_8$ (d)	30-600	21	2	5	7	n/d	n/d	n/d	–	n/d	–	28	Krzhizhanovskaya *et al.*, 2012
$NaAlSi_3O_8$ (d)	25–970	n/d	n/d	n/d	n/d	16.2	6.2	2.4	n/d	n/d	n/d	29.6	Winter, 1977
$NaAlSi_3O_8$ (o)	24–1060	n/d	n/d	n/d	n/d	13.1	8.5	4.5	n/d	n/d	n/d	29.6	Winter, 1979
$NaBSi_3O_8$ (o)	30–	22	7	-0.2	n/d	n/d	n/d	n/d	n/d	n/d	n/d	n/d	Derkacheva *et al.* 2017

https://doi.org/10.1180/mgm.2025.6 Published online by Cambridge University Press

$LiAlSi_3O_8$ (o)	600 – 526	35.1(1)	-5.9(9)	10.9(9)	56.9(8)	10.8(8)	14.6(1)	10(1)	-20.2(8)	0.4(5)	-2.8(8)	40(2)	Hovis *et al.*, 2008***

* $\mu_{(\alpha 33 \wedge c)}$ show the orientation angle between the α_{11} and *c* axis
** (d) and (o) indicate disordered and ordered crystal structures, respectively
*** TECs are calculated based on the original data
n/d – no data available

The volume thermal expansion (α_V) of $RbAlGe_3O_8$ is slightly higher compared to its alumino- and galliumsilicates, but lower than borosilicates analogues (Table 3). Besides, if the feldspar-related compound has ordered (o) and disordered (d) modifications, their volume and linear TECs are practically similar (Hovis *et al.,* 2008). It should be noted that for the sake of comparison the volume TECs, discussed here, are calculated using the linear approximation model and does not consider the fact that variations of α_V with temperature is typical for feldspars (Tribaudino *et al.,* 2010). At the same time, $RbAlGe_3O_8$ has the largest unit-cell volume among other alkaline feldspars (Table 2). It is traditionally believed that feldspars with larger unit cell expand less upon heating (Hovis *et al*., 2008), that contradicts the result obtained in this study. This discrepancy may be due to the fact that the statement by Hovis *et al*. (2008) is formulated for feldspar with aluminosilicate framework and does not consider isostructural compounds with other composition of the framework. Nevertheless, the linear TECs and the general trends of thermal expansion are very close for all of them (Table 3). The K-borosilicate alkali feldspar example has the highest α_V in the series, and exhibits the least anisotropy. We can see that volume thermal expansion (Table 3) of alkali feldspars decreases with the increasing of the cation size (from Li (0.92 Å) to Rb (1.66 Å); Shannon, 1976). Interestingly, this dependence is inverse for alkaline earth feldspars with paracelsian topology, i.e. the volume thermal expansion increases with the increasing size of extra-framework cations (Gorelova *et al.*, 2015; Gorelova, 2023). High temperature behavior of $RbAlGe_3O_8$ is also consistent with the main

https://doi.org/10.1180/mgm.2025.6 Published online by Cambridge University Press

factor controlling the thermal expansion being the framework topology rather than the extra-framework or framework-forming cations (Angel *et al.*, 2012).

4. Conclusion

The experiments on synthesis of the Ge analogue of rubicline showed that it forms at similar temperatures and via similar stages as rubicline: both compounds are formed in hydrothermal conditions after crystallization of a leucite/pollucite-like Rb-rich phase. The crystal structure of synthetic $RbAlGe_3O_8$, obtained during this work (as well as other synthetic alkaline feldspars) is Ge / Al disordered, whereas natural rubicline was found to occur in both ordered and disordered crystal structures. The high temperature behavior of $RbAlGe_3O_8$ is typical for feldspar-related minerals with feldspar topology, i.e. it is quite anisotropic. Obtaining experimental data on the thermal behavior of feldspars with different framework-forming cations will make it possible to create a model for predicting thermal expansion coefficients for feldspars with all possible chemical compositions.

Acknowledgments: The authors thank X-ray Diffraction Centre and Geomodel Centre of Saint Petersburg State University for providing instrumental and computational resources. This research was funded by the Russian Science Foundation, grant number 22-77-10033 (to L.A.G., V.A.Y. and O.S.V.).

Competing interests: The authors declare none.

References

Agilent. (2012) CrysAlis PRO. Agilent Technologies, Oxfordshire, UK.

Ahrens, T.J., Petersen, C.F. and Rosenberg, J.T. (1969) Shock compression of feldspars. *Journal of Geophysical Research*, **74**, 2727–2746.

Angel, R.J. (1994) Feldspars at high pressure. Pp. 271–312 in: *Feldspars and Their Reactions* (I. Parsons, editor). Springer, Dordrecht.

https://doi.org/10.1180/mgm.2025.6 Published online by Cambridge University Press

Angel, R.J., Sochalski-Kolbus, L.N. and Tribaudino M. (2012) Tilts and tetrahedra: The origin of the anisotropy of feldspars. *Am. Mineral*., **97**, 765–778.

Appiah, M., Yang, Y., Ullah, B., Xiao, Y., Stavrou, E., Zhang, Q. and Tan, D.Q. (2024) Phase structural characteristics and microwave dielectric properties of Ge-doped cordierite-based ceramics. *Materials Research Bulletin*, **179**, 112939.

De Argollo, R. and Schilling, J.G. (1978) Ge-Si and Ga-Al fractionation in Hawaiian volcanic rocks. *Geochimica et Cosmochimica Acta*, **42**, 623–630.

Baronas, J.J., Torres, M.A., West, A.J., Rouxel, O., Georg, B., Bouchez, J., Gaillardet, J. and Hammond, D.E. (2018) Ge and Si isotope signatures in rivers: A quantitative multi-proxy approach. *Earth and Planetary Science Letters*, **503**, 194–215. Elsevier B.V.

Barrer, R.M. and Baynham, J.W. (1956) The hydrothermal chemistry of the silicates. Part VII. Synthetic potassium aluminosilicates. *Journal of the Chemical Society (Resumed)*, 2882–2891.

Barrer, R.M. and McCallum, N. (1953) Hydrothermal chemistry of silicates. Part IV. Rubidium and cœsium aluminosilicates. *Journal of the Chemical Society (Resumed)*, 4029–4035.

Barry Carter, C. and Grant Norton, M. (2008) Ceramic materials. New York (NY): Springer.;

Bell, A.M.T. (2024) Crystal structures and X-ray powder diffraction data for $AAlGe_2O_6$ synthetic leucite analogs (A = K, Rb, Cs). *Powder Diffraction*, **39**, 162–169.

Bernstein, L.R. (1985) Germanium geochemistry and mineralogy. *Geochimica et Cosmochimica Acta*, **49**, 2409–2422.

Bokiy, G.B. and Borutzky, B.Y. (2003) *Minerals. Vol.5: Silicates with interrupted framework, feldspar minerals*. P. in.: Nauka, Moscow, 583 pp.

Breck, D.W. (1974) *Zeolite Molecular Sieves: Structure, Chemistry and Use*. P. in.: John Wiley, New York, 771 pp.

Brown, L.B., Openshaw, R.E., McMillan, P.F. and Henderson, C.M.B (1984) A review of the expansion of alkali feldspars: coupled variations in cell parameters and possible phase transitions. *Am. Mineral*., **69**, 1058–1071.

Bruno, E. and Pentinghaus, H. (1974) Substitutions of cations in natural and synthetic feldspars. Pp. 574–610 in: *The Feldspars* (W.S. Mackenzie and J. Zussmann, editors). Manchester University Press, Manchester.

Bubnova, R.S., Firsova, V.A. and Filatov, S.. (2013) Software for determining the thermal expansion tensor and the graphic representation of its characteristic surface (Theta to Tensor-TTT). *Glass Physics and Chemistry*, **39**, 347–350.

Butterman, W.C. and Reese, R.G.J. (2003) *Mineral Commodity Profiles -- Rubidium*. Version 1. 11 pp.

Cheng, C.H., Juttu, G., Mitchell, S.F. and Shantz, D.F. (2006) Synthesis, characterization, and growth rates of germanium silicalite-1 grown from clear solutions. *Journal of Physical Chemistry B*, **110**, 21430–21437.

Christy, A.G. (2015) Causes of anomalous mineralogical diversity in the Periodic Table. *Mineralogical Magazine*, **79**, 33–49.

Colville, A.A. and Ribbe, P.H. (1968) The crystal structure of an adularia and a refinement of the structure of orthoclase. *American Mineralogist*, **53**, 25–37.

https://doi.org/10.1180/mgm.2025.6 Published online by Cambridge University Press

Corma, A., Martín-Aranda, R.M. and Sánchez, F. (1990) Zeolites as base catalysts: Condensation of benzaldehyde derivatives with activated methylenic compounds on Germanium-substituted faujasite. *Journal of Catalysis*, **126**, 192–198.

Deer, W.A., Howie, R.A. and Zusmann, J. (2001) *Rock-Forming Minerals. Vol. 4A. Framework Silicates: Feldspars*. P. in.: The Geological Society, London, 973 pp.

Deer, W.A., Howie, R.A. and Zussman, J. (2013) *An Introduction to the Rock-Forming Minerals, 3d ed.* P. in.: Mineralogical Society of Great Britain and Ireland, 696 pp.

Derkacheva, E.S., Krzhizhanovskaya, M.G. and Bubnova, R.S. (2017) Thermal behavior of reedmergnerite $NaBSi_3O_8$ and searlesite $NaBSi_2O_5(OH)_2$. *Glass Physics and Chemistry*, **43**, 459–463.

Dinnebier, R.E., Leineweber, A. and Evans, J.S.O. (2019) *Rietveld Refinement: Practical Powder Diffraction Pattern Analysis using TOPAS*. P. in.: De Gruyter, Berlin, Boston, 331 pp.

Ferguson, R.B., Ball, N.A. and Cerny, P. (1991) Structure refinement of an adularian end-member high sanidine from the Buck Claim pegmatite, Bernic Lake, Manitoba. *The Canadian Mineralogist*, **29**, 543–552.

Filatov, S.K. (1971) Anomale Wärmeausdehnung von V2O5. *Crystal Research and Technology*, **6**, 777-785 [in German].

Filatov, S.K. (1990) *High-Temperature Crystal Chemistry*. P. in.: Nedra, Leningrad [in Russian].

Froelich, P.N., Blanc, V., Mortlock, R.A., Chillrud, S.N., Dunstan, W., Udomkit, A. and Peng, T.-H. (1992) River fluxes of dissolved silica to the ocean were higher during glacials: Ge/Si in diatoms, rivers, and oceans. *Paleoceanography*, **7**, 739–767.

Fuertes, V., Reinosa, J.J., Fernandez, J.F. and Enriquez E. (2022) Engineered feldspar-based ceramics: A review of their potential in ceramic industry. *J. Eur. Ceram. Soc*., **42**, 307–326.

Gasperin, M. (1971) Structure cristalline de $RbAlSi_3O_8$. *Acta Crystallographica*, **27**, 854–855.

Ghelis, M. and Gasperin, M. (1970) Evolution des parametres dans le systeme $KalSi_3O_8$–$RbAlSi_3O_8$. *Comptes rendus de l'Académie des Sciences*, **271**, 1928-1929 [in French].

Goldschmidt, V.M. (1926) Über das krystallochemische und geochemische Verhalten des Germaniums. *Naturwissenschaften*, **14**, 295-297 [in German].

Goldschmidt, V.M. (1958) *Geochemistry*. P. in.: Oxford University Press, London, 425 pp.

Gorelova, L.A. (2023) Phase transformations in feldspar group minerals with paracelsian topology under high temperature and high pressure. *Russian Geology and Geophysics*, **64**, 950–961.

Gorelova, L.A., Filatov, S.K., Krzhizhanovskaya, M.G. and Bubnova, R.S. (2015) High-temperature behavior of danburite-like borosilicates $MB_2Si_2O_8$ (M = Ca, Sr, Ba). *Physics and Chemistry of Glasses*, **56**, 189–196.

Gorelova, L.A., Vereshchagin, O.S., Bocharov, V.N., Potekhina (née Shchipalkina), N. V., Zhitova, E.S. and Pekov, I. V. (2024) Thermal behaviour of filatovite – a rare aluminoarsenate mineral of the feldspar group. *Mineralogical Magazine*, **88**, 176–184.

Greenwood, N.N., and Earnshaw, A. (1998), Chap. 4, Lithium, sodium, potassium, rubidium, caesium and francium, in Chemistry of the elements (2d ed.): Oxford, United Kingdom, Butterworth-Heinemann, 1, 341 p.

https://doi.org/10.1180/mgm.2025.6 Published online by Cambridge University Press

Grove, T. and Ito, J. (1973) High temperature displacive transformations in synthetic feldspar. *Transactions of the American Geophysical Union*, **54**, 499.

Helliwell, M., Kaučič, V., Cheetham, G.M.T., Harding, M.M., Kariuki, B.M. and Rizkallah, P.J. (1993) Structure determination from small crystals of two aluminophosphates CrAPO-14 and SAPO-43. *Acta Crystallographica Section B*, **B49**, 413–420. International Union of Crystallography.

Henderson, C.M.B. (1978) The thermal expansion of synthetic aluminosilicate-sodalites, $M_8(Al_6Si_6O_{24})_{X2}$. *Physics and Chemistry of Minerals*, **2**, 337–347.

Henderson, C.M.B. (2021) Composition, thermal expansion and phase transitions in framework silicates: revisitation and review of natural and synthetic analogues of nepheline-, feldspar- and leucite-mineral groups. *Solids*, **2**, 1–49. Multidisciplinary Digital Publishing Institute (MDPI).

Henderson, C.M.B., Bell, A.M.T. and Knight, K.S. (2017) Variable stoichiometry in tectosilicates having the leucite/pollucite-type structure with particular emphasis on modelling the interframework cavity cation environment. *Journal of Solid State Chemistry*, **251**, 90–104. Elsevier Inc.

Hovis, G.L., Morabito, J.R., Spooner, A., Mott, A., Person, E.L., Henderson, C.M.B., Roux, J. and Harlov, D. (2008) A simple predictive model for the thermal expansion of $AlSi_3$ feldspars. *Am. Mineral.*, **93**, 1568–1573.

Kimata, M., Saito, S. and Shimizu, M. (1995) Structure of sanidine-type $KGaSi_3O_8$: Tetrahedral-site disordering in potassium feldspar. *European Journal of Mineralogy*, **7**, 287–294.

Kimball, M.R. and Megaw, H.D. (1974) Interim report on the crystal structure of buddingtonite. Pp. 81–86 in: *The Feldspars. Proceedings of the NATO ASI on Feldspars* (W.S. MacKenzie and J. Zussman, editors). Manchester University Press, Manchester.

Kinomura, N., Koizumi, M. and Kume, S. (1971) Germanate alkali feldspars under pressure. *Journal of Geophysical Research*, **76**, 2035–2037.

Kirkpatrick, R.J., Klein, L., Uhlmann, D.R. and Hays, J.F. (1979) Rates and processes of crystal growth in the system anorthite-albite. *Journal of Geophysical Research: Solid Earth*, **84**, 3671–3676.

Kivlighn, H.D. (1966) Solid state reactivity and glass crystallization behavior of some alkali aluminogermanates. *Journal of the American Ceramic Society*, **49**, 148–151.

Kovalev, V.N., Spivak, A. V, Setkova, T. V, Ksenofontov, D.A., Volkova, E.A., Korepanov, V.I., Balitsky, V.S. and Zakharchenko, E.S. (2024) High-pressure Raman spectroscopy study of α-quartz-like $Si_{1-x}Ge_xO_2$ solid solution. *Journal of Physics and Chemistry of Solids*, **185**, 111749.

Kovalskii, A.M., Kotel'nikov, A.R., Bychkov, A.M., Chichagov, A.V. and Samokhvalova, O.L. (2000) Synthesis and X-ray diffraction study of (K, Rb)-feldspar solid solution: preliminary data. *Geochemistry International*, **38**, 220–224.

Krivovichev, S. V. (2020) Feldspar polymorphs: diversity, complexity, stability. *Zapiski Rossiiskogo Mineralogicheskogo Obshchestva*, **149**, 16–66.

Kroll, H. and Ribbe, P. (1987) Determining (Al,Si) distribution and strain in alkali feldspars using lattice parameters and diffraction-peak positions; a review. *American Mineralogist*, **72**, 491–506.

https://doi.org/10.1180/mgm.2025.6 Published online by Cambridge University Press

Kroll, H., Floegel, J., Breit, U., Loens, J. and Pentinghaus, H. (1991) Order and anti-order in Ge-substituted alkali feldspars. *European Journal of Mineralogy*, **3**, 739–749.

Krzhizhanovskaya, M.G., Bubnova, R.S., Depmeier, W., Rahmoun, N.S., Filatov, S.K. and Ugolkov, V.L. (2012) A new borosilicate feldspar, $KBSi_3O_8$: synthesis, crystal structure and thermal behavior. *Zeitschrift fur Kristallographie - Crystalline Materials*, **227**, 446–451.

Kume, S., Matsumoto, T. and Koizumi, M. (1966) Dense form of germanate orthoclase ($KAlGe_3O_8$). *Journal of Geophysical Research*, **71**, 4999–5000.

Kume, S., Ueda, S. and Koizumi, M. (1969) Synthesis and phase change of germanate albite under pressures. *Journal of Geophysical Research*, **74**, 2145–2147.

Kurtz, A.C., Derry, L.A. and Chadwick, O.A. (2002) Germanium-silicon fractionation in the weathering environment. *Geochimica et Cosmochimica Acta*, **66**, 1525–1537.

Kyono, A. and Kimata, M. (2001) Refinement of the crystal structure of a synthetic non-stoichiometric Rb-feldspar. *Mineralogical Magazine*, **65**, 523–531.

Lerot, L., Poncelet, G. and Fripiat, J.J. (1975) Surface and some catalytic properties of a germanic near-faujasite molecular sieve. *Journal of Solid State Chemistry*, **12**, 283–287.

Li, H. and Yaghi, O.M. (1998) Transformation of Germanium Dioxide to Microporous Germanate 4-Connected Nets. *Journal of the American Chemical Society*, **120**, 10569–10570.

Liu, C., Komarneni, S. and Roy, R. (1994) Seeding effects on crystallization of $KAlSi_3O_8$, $RbAlSi_3O_8$, and $CsAlSi_3O_8$ gels and glasses. *Journal of the American Ceramic Society*, **77**, 3105–3112.

McMillan, P.F., Brown, W.L. and Openshaw, R.E. (1980) The unit-cell parameters of an ordered K-Rb alkali feldspar series. *American Mineralogist*, **65**, 458–464.

McMillan, P.W. (1979) *Glass-ceramics*. P. in.: Academic Press, Information London ; New Yor, 285 pp.

Megaw, H.D. (1974) The architecture of feldspars. Pp. 2–24 in: *The Feldsparsi* (W.S. AcKenzie and J. Zussman, editors). Manchester University Press, Manchester, UK.

Mortlock, R.A. and Frohlich, P.N. (1987) Continental weathering of germanium: Ge/Si in the global river discharge. *Geochimica et Cosmochimica Acta*, **51**, 2075–2082.

Murnane, R.J. and Stallard, R.F. (1990) Germanium and silicon in rivers of the Orinoco drainage basin. *Nature*, **344**, 749–752.

O'Keeffe, M. and Yaghi, O.M. (1999) Germanate Zeolites: Contrasting the Behavior of Germanate and Silicate Structures Built from Cubic T_8O_{20} Units (T=Ge or Si). *Chemistry – A European Journal*, **5**, 2796–2801.

Ohtake, M., Matsunaga, T., Haruyama, J., Yokota, Y., Morota, T., Honda, C., Ogawa, Y., Torii, M., Miyamoto, H., Arai, T., Hirata, N., Iwasaki, A., Nakamura, R., Hiroi, T., Sugihara, T., Takeda, H., Otake, H., Pieters, C.M., Saiki, K., Kitazato, K., Abe, M., Asada, N., Demura, H., Yamaguchi, Y., Sasaki, S., Kodama, S., Terazono, J., Shirao, M., Yamaji, A., Minami, S., Akiyama, H. and Josset, J.L. (2009) The global distribution of pure anorthosite on the Moon. *Nature*, **461**, 236–240. Nature Publishing Group.

Pekov, I. V, Kononkova, N.N., Agakhanov, A.A., Belakovskiy, D.I., Kazantsev, S.S. and Zubkova, N. V. (2009) Voloshinite, a new rubidium mica from granite pegmatites of Voron'i Tundras (Kola Peninsula). *Zapiski Rossiiskogo Mineralogicheskogo Obshchetstva*,

https://doi.org/10.1180/mgm.2025.6 Published online by Cambridge University Press

138, 90-100 [in Russian].

Pentinghaus, H. and Bambauer, H. (1971) Substitution of Al(III), Ga(III), Fe(III), Si(IV) and Ge(IV) in synthetic alkali feldspars. *Neues Jahrbuch für Mineralogie - Monatshefte*, 416–418.

Rainer, T., Paul, D. and Hahn, A. (2008) Ramanite-(Cs) and ramanite-(Rb): New cesium and rubidium pentaborate tetrahydrate minerals identified with raman spectroscopy. *American Mineralogist*, **93**, 1034–1042.

Ralph, J., Von Bargen, D., Martynov, P., Zhang, J., Que, X., Prabhu, A., Morrison, S.M., Li, W., Chen, W. and Ma, X. (2024) Author and Article Information. *American Mineralogist* https://doi.org/10.2138/am-2024-9486

Ringwood, A.E., Reid, A.F. and Wadsley, A.D. (1967) High pressure transformation of alkali aluminosilicates and aluminogermanates. *Earth and Planetary Science Letters*, **50**, 38–40.

Schairer, J.F. and Bowen, N.L. (1955) The system K_2O-Al_2O_3 -SiO_2. *American Journal of Science*, **253**, 681–746.

Shannon, R.D. (1976) Revised effective ionic radii and systematic studies of interatomic distances in halides and chalcogenides. *Acta Crystallographica*, **A32**, 751–767.

Sheldrick, G.M. (2008) A short history of SHELX. *Acta Crystallographica Section A*, **64**, 112–122. International Union of Crystallography.

Silva, A.C., Carolina, S.D., Sousa, D.N. and Silva E.M.S. (2019) Feldspar production from dimension stone tailings for application in the ceramic industry. *J Mater Res Technol*., **8**, 1–7.

Smith, J. V. and Brown, W.L. (1988) *Feldspar Minerals. Volume 1 Crystal Structures, Physical, Chemical, and Microtextural Properties*. P. in.: Springer Verlag, Berlin Heidelberg, 828 pp.

Smith, J.V. (1958) Further discussion of framework structures formed from parallel four-and eight-membered rings. *Mineralogical Magazine*, **33**, 202–212.

Smith, J.V. (1974) *Feldspar Minerals. I. Crystal Structure and Physical Properties*. P. in.: Springer-Verlag, Berlin, 627 pp.

Solodov, N.A., Balashov, L.S. and Kremenetsky, A.A. (1980) *Geochemistry of Lithium, Rubidium, and Cesium*. P. in.: Nedra, Moscow, 234 [in Russian] pp.

Suzuki, R., Takahashi, Y., Iwasaki, K., Terakado, N. and Fujiwara, T. (2015) High thermal stability of red emission in Mn-doped benitoite-type strontium silicogermanate. *Applied Physics Express*, **8**, 72603. The Japan Society of Applied Physics.

Taylor, M. and Brown, G.E. (1979) Structure of mineral glasses-I. The feldspar glasses $NaAlSi_3O_8$, $KAlSi_3O_8$, $CaAl_2Si_2O_8$. *Geochimica et Cosmochimica Acta*, **43**, 61–75.

Teertstra, D.K., Černý, P. and Hawthorne, F.C. (1997) Rubidium-rich feldspars in a granitic pegmatite from the Kola Peninsula, Russia. *Canadian Mineralogist*, **35**, 1277–1281.

Teertstra, D.K., Černý, P., Hawthorne, F.C., Pier, J., Wang, L.M. and Ewing, R.C. (1998a) Rubicline, a new feldspar from San Piero in Campo, Elba, Italy. *American Mineralogist*, **83**, 1335–1339.

Teertstra, D.K., Černý, P. and Hawthorne, F.C. (1998b) Rubidium-rich feldspars and associated minerals from the Luolamaki pegmatite, Somero, Finland. *Bulletin of the Geological Society of Finland*, **70**, 43–49.

https://doi.org/10.1180/mgm.2025.6 Published online by Cambridge University Press

Teertstra, D.K., Černý, P. and Hawthorne, F.C. (1998c) Rubidium feldspars in granitic pegmatites. *Canadian Mineralogist*, **36**, 483–496.

Teertstra, D.K., Černý, P. and Hawthorne, F.C. (1999a) Geochemistry and petrology of late K- and Rb-feldspars in the Rubellite pegmatite, Lilypad Lakes, NW Ontario. *Mineralogy and Petrology*, **65**, 237–247.

Teertstra, D.K., Černý, P. and Hawthorne, F.C. (1999b) Subsolidus rubidium-dominant feldspar from the Morrua pegmatite, Mozambique: paragenesis and composition. *Mineralogical Magazine*, **63**, 313–320.

Terry, R.J., Vinton, D., McMillen, C.D., Chen, X., Zhu, L. and Kolis, J.W. (2022) Hydrothermal single crystal growth and structural investigation of the stuffed tridymite family as NLO materials. *Journal of Alloys and Compounds*, **909**, 164634.

Torres-Martinez, L.M. and West, A.R. (1989) Pollucite- and Leucite-related phases: $A_2BX_5O_{12}$ and ACX_2O_6 (A = K, Rb, Cs; B = Be, Mg, Fe, Co, Ni, Cu, Zn, Cd; C = B, Al, Ga, Fe, Cr; X = Si, Ge). *Zeitschrift für anorganische und allgemeine chemie*, **573**, 223–230.

Tribaudino, M., Angel, R.J., Camara, F., Nestola, F., Pasqual, D. and Margiolaki, I. (2010) Thermal expansion of plagioclase feldspars. *Contrib. Mineral. Petrol.*, **160**, 899–908.

Tribaudino, M., Bruno, M., Nestola, F., Pasqual, D. and Angel, R.J. (2011) Thermoelastic and thermodynamic properties of plagioclase feldspars from thermal expansion measurements. *American Mineralogist*, **96**, 992–1002.

Tripathi, A. and Parise, J.B. (2002) Hydrothermal synthesis and structural characterization of the aluminogermanate analogues of JBW, montesommaite, analcime and paracelsian. *Microporous and Mesoporous Materials*, **52**, 65–78.

Vadawale, S. V, Mithun, N.P.S., Shanmugam, M., Basu Sarbadhikari, A., Sinha, R.K., Bhatt, M., Vijayan, S., Srivastava, N., Shukla, A.D., Murty, S.V.S., Bhardwaj, A., Acharya, Y.B., Patel, A.R., Adalaja, H.L., Vaishnava, C.S., Saiguhan, B.S.B., Singh, N., Kumar, S., Painkra, D.K., Srivastava, Y., Nair, V.M., Ladiya, T., Goyal, S.K., Tiwari, N.K., Narendranath, S., Pillai, N.S., Hait, A.K., Patinge, A., Kumar, A., Satya, N., Subramanian, V.R., Navle, S.G., Venkatesh, R.G., Abraham, L., Suresh, K. and Amitabh. (2024) Chandrayaan-3 APXS elemental abundance measurements at lunar high latitude. *Nature*, **633**, 327–331.

Voncken, J. (1996) Crystal morphology and X-ray powder diffraction of the Rb-analogue of high sanidine $RbAlSi_3O_8$. *Neues Jahrbuch für Mineralogie - Monatshefte*, **1**, 10–16.

Wietze, R. and Wiswanathan, K. (1971) Rubidium-plagioklas durch kationenaustauch. *Fortschr. Miner*, **49**, 63 [in German].

Winter, J.K., Ghose, S. and Okamura, F.P. (1977) A high-temperature study of the thermal expansion and the anisotropy of the sodium atom in low albite. *American Mineralogist*, **62**, 921–931.

Winter, J.K., Okamura, F.P. and Ghose, S. (1979) A high-temperature structural study of high albite, monalbite, and the analbite-monalbite phase transition. *American Mineralogist*, **64**, 409–423.

Xing, P., Wang, C., Ma, B., Wang, L., Zhang, W. and Chen, Y. (2018) Rubidium and Potassium Extraction from Granitic Rubidium Ore: Process Optimization and Mechanism Study. *ACS Sustainable Chemistry and Engineering*, **6**, 4922–4930.

Zhang, L., Mei, H., Rao, Z., Shu, L. and Li, C. (2022) Lowered sintering temperature and

https://doi.org/10.1180/mgm.2025.6 Published online by Cambridge University Press

modulated microwave dielectric properties in Mg_2SiO_4 forsterite via Ge substitution. *Journal of Materials Science: Materials in Electronics*, **33**, 10183–10193.

Zhang, Y., Hu, Y., Sun, N., Jiu, R., Wang, Z., Wang, L. and Sun W. (2018) Systematic review of feldspar beneficiation and its comprehensive application. *Minerals Engineering*, **128**, 141–152.

https://doi.org/10.1180/mgm.2025.6 Published online by Cambridge University Press